communications biology

A Nature Portfolio journal

Article

https://doi.org/10.1038/s42003-025-08873-4

Edge participation coefficient unveiling the developmental dynamics of neonatal functional connectome

Tianyu Fang[1,2,3,4], Rong Wang[1,2,3,4], Weijin Liu[1,2,3,4], Yue Zhang[1,2,3,4], Yu Guo[1,2,3,4], Yichen Hu[1,2,3,4], Xin Zhao[1,2,3,4], Yuanyuan Chen[1,2,3,4] ✉, Qiuyun Fan[1,2,3,4] ✉ & Dong Ming[1,2,3,4] ✉

Understanding how the brain's functional connections develop during infancy is crucial for uncovering the complexities of early neural maturation. Traditional node-based analyses have advanced our knowledge, but may overlook the transient dynamics of interregional connectivity. Leveraging the large neonatal functional MRI dataset from the Developing Human Connectome Project (n = 781, including 494 full-term and 287 preterm infants), we introduce an edge-centric metric to quantify cross-module functional integration. Here we show that preterm infants exhibit higher edge participation coefficients than full-term peers, suggesting delayed network specialization. We mapped developmental changes in edge participation coefficients and found that between-network connections—particularly those involving visual and higher-order systems—undergo the most pronounced changes and are associated with cognitive outcomes at 18 months. By analyzing gene expression in a developing brain, we identified genes involved in neurodevelopmental processes and cellular signalling that may underlie these patterns. Our findings illustrate how interregional diversity evolves in early life and provide insight into the molecular basis of early brain development.

The early postnatal period represents a critical window for brain network maturation, during which deviations in functional connectivity trajectories are strongly linked to neurodevelopmental disorders such as cerebral palsy and autism spectrum disorders[1–3]. However, the dynamic principles governing connectome refinement in infancy—particularly in high-risk populations like preterm infants—remain poorly characterized, limiting early intervention strategies. The early brain undergoes rapid synaptogenesis, establishing a dense network of potential neural connections, which, through the processes of synaptic pruning, are subsequently refined by environmental stimuli and genetic factors[4–6]. These findings have not only provided insights into the mechanisms underlying neural plasticity but have also underscored the dynamic and adaptive nature of early brain development.

Advancements in neuroimaging and computational modeling have illuminated the developmental transition from a brain with generalized, diffuse connections to one characterized by increased specificity and modular organization. This shift marks a critical juncture where the connectome begins to mirror the sophisticated architecture observed in adulthood, indicative of its readiness for more complex information processing tasks[7,8]. It is during these stages that neural hubs begin to assert their influence, acting as integrative centers that bind disparate regions of the brain into a cohesive, functioning whole. These hubs not only become more interconnected but also more selective in their connections, paralleling the neonate's own maturation and emerging cognitive capacities[9,10].

Actually, infancy is characterized by a remarkable surge in synaptic connections, followed by a selective pruning process, an essential sequence for shaping efficient neural networks and supporting cognitive and behavioral refinement. This period of exuberant synaptogenesis is evidenced by studies showing a rapid increase in synaptic density in various regions of the brain, most notably in the cortex[11,12]. This synaptic overproduction, observed in the early months of life, sets the stage for extensive neural connectivity, allowing the infant brain to adapt to and learn from its environment with remarkable efficiency[13,14]. Subsequently, synaptic pruning becomes a pivotal process in later infancy and early childhood. This phase involves the elimination of less active synapses, an activity-dependent process that refines brain circuitry for optimal function. This dynamic interplay between synaptic growth and pruning underlines the brain's developmental plasticity during infancy, shaping the emerging functional connectome in response to both intrinsic developmental programs and external stimuli[15–18]. By examining these edges and their dynamic

[1]Medical School, Faculty of Medicine, Tianjin University, Tianjin, China. [2]State Key Laboratory of Advanced Medical Materials and Devices, Tianjin University, Tianjin, China. [3]Haihe Laboratory of Brain-Computer Interaction and Human-Machine Integration, Tianjin, China. [4]Tianjin Key Laboratory of Brain Science and Neuroengineering, Tianjin, China. ✉e-mail: bain@tju.edu.cn; fanqiuyun@tju.edu.cn; richardming@tju.edu.cn

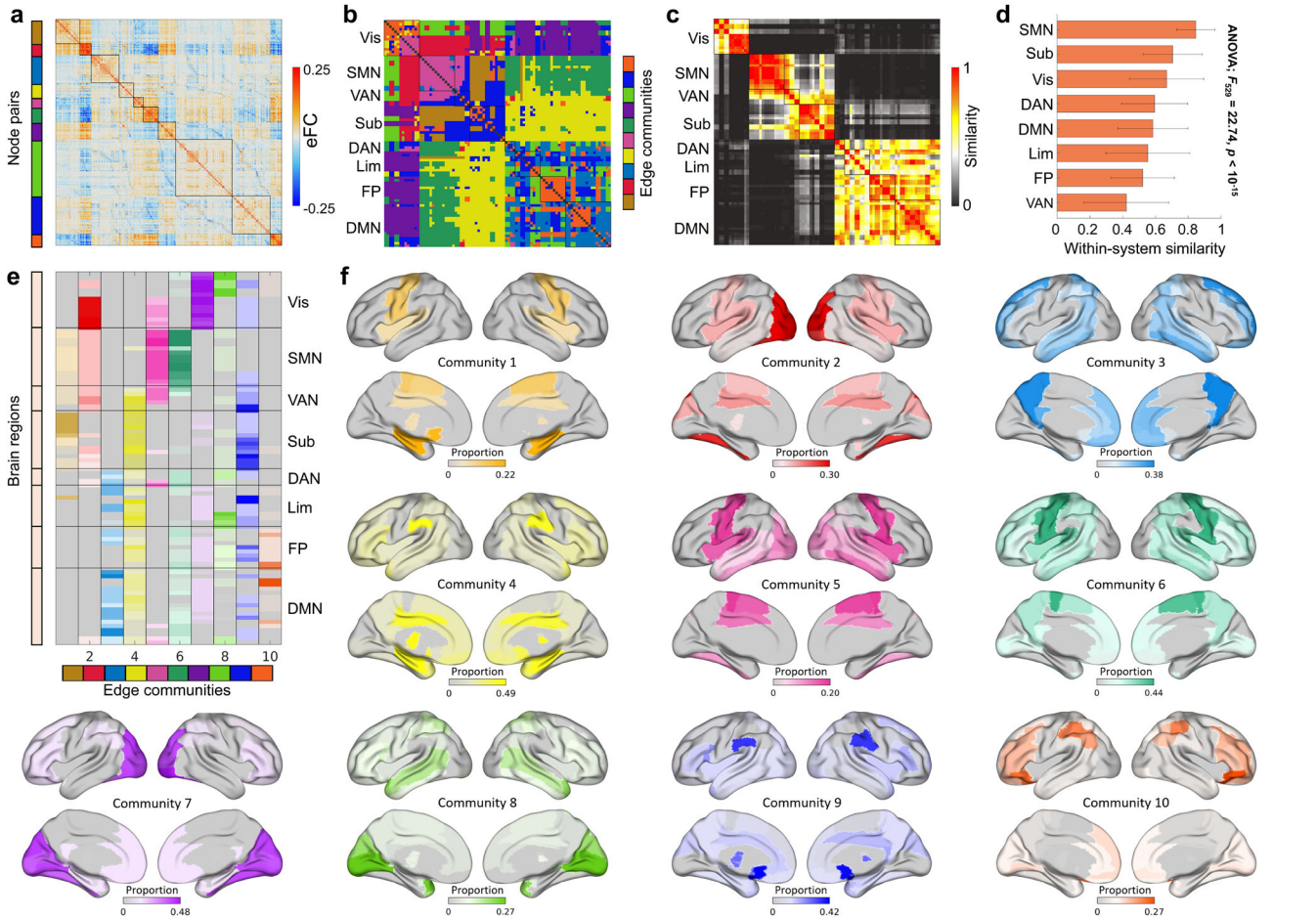

Fig. 1 | The overlapping community structure of the cerebral cortex in term-born infants. a The eFC matrix is reordered according to the detected ten communities. **b** Edge community labels in matrix form. **c** The similarity of edge community assignments associated with the two connected regions. **d** Comparison of within-system similarity values for each of the 8 pre-defined brain systems (ANOVA; $F_{529} = 22.74$, $P < 10^{-15}$). All error bars indicate standard errors of the mean. **e** Proportion of all edges assigned to each community that included a given node as one of its endpoints. **f** Topographic distribution of communities by overlaying the proportions onto a brain surface using BrainNet Viewer[95].

fluctuation patterns, new perspectives could be gained on how the brain reconfigures itself, potentially unlocking new dimensions of understanding about functional connectome organization and development.

The interplay between genetic programming and environmental influences in shaping early brain development has long been conceptualized as a linear, additive process, with studies focusing on isolated molecular pathways or structural anomalies as static predictors of neurodevelopmental outcomes[19]. However, studies revealed that structural metrics alone poorly predict long-term cognitive trajectories in preterm infants[20], while dynamic functional connectivity patterns, particularly in default-mode networks, show striking prognostic value for 18-month outcomes[21]. This discrepancy underscores a critical gap: current models fail to reconcile how molecular mechanisms (e.g., activity-dependent gene expression) dynamically interact with environmental stressors (e.g., preterm extrauterine exposure) to drive edge-level network reconfiguration. Single-scale approaches dominate the field, with neuroimaging studies rarely bridging transcriptomic signatures to functional dynamics, and vice versa, which identified regional white matter variations shaped by gene-environment interactions but lacked mechanistic links to functional plasticity[22].

Despite significant advances in understanding early connectome maturation, most existing approaches remain node-centric[23–27], focusing on the roles of brain regions while overlooking the dynamic interactions between them. However, emerging evidence suggests that critical aspects of functional reorganization occur at the level of individual connections (edges), rather than solely at the level of brain regions (nodes). Recently, Faskowitz et al.[28] proposed an edge-centric model to represent pairwise functional interactions among a network's edges, which offers a distinct yet complementary insight into brain network organization and operation, compared with traditional node-based functional connectivity (nFC). Whereas nFC measures the extent to which the activity of one brain region fluctuates with the activity of another, eFC unwraps those co-fluctuations across time, first yielding moment-by-moment accounts of the co-fluctuations between pairs of brain regions (edges) and then assessing the similarity between the time series of these co-fluctuations[29]. Although both nFC and eFC are derived from the identical fMRI time series, eFC provides unique insights into dynamic network reconfiguration and has been increasingly recognized to be more sensitive to individual idiosyncrasies in brain organization[28–33]. Nevertheless, quantitative metrics that characterize the dynamic roles of edges across functional modules remain under-explored, particularly in infant populations, where developmental plasticity is most pronounced. This heightened sensitivity to dynamic reconfiguration makes edge-centric analysis particularly well-suited for probing the rapidly evolving and highly plastic functional networks of the neonatal brain.

To address these limitations, we aim to characterize early development of functional connectome organization at the level of individual connections by applying an edge-centric analytic framework to resting-state fMRI data in preterm and term-born infants. We introduce the edge-centric participation coefficient (ePC) to quantify the functional diversity of each connection and assess its relationship with neurodevelopmental outcomes and transcriptomic signatures. This edge-centric approach enables a more granular

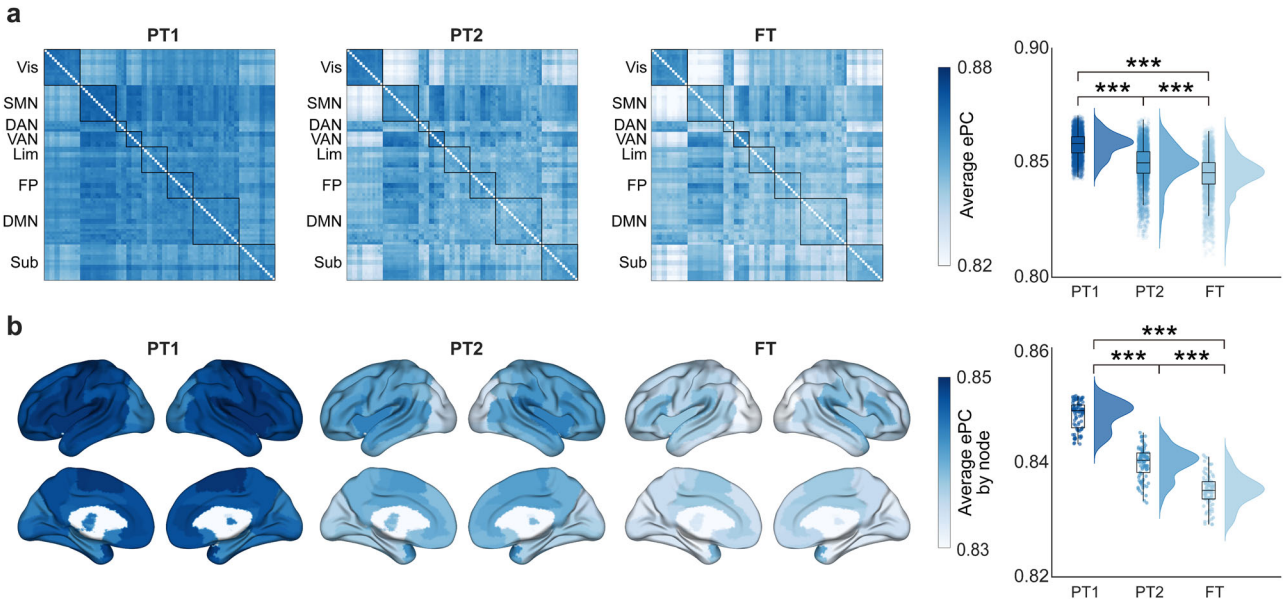

Fig. 2 | Edge PC patterns at both the regional and edge-wise level. a The average edge PC pattern at the edge level for each group (PT1: preterm infants scanned at birth; PT2: preterm infants scanned at term-equivalent age; FT: full-term infants scanned at birth), along with a comparison of their whole-brain distributions illustrated on the right, with each point representing an edge (4005 edges for each group). Pairwise comparisons of these distributions were performed using two-sample t-tests, with *P*-values FDR-corrected for multiple comparisons using the Benjamini–Hochberg method (*$P < 0.05$; **$P < 0.01$; ***$P < 0.001$). **b** The average edge PC pattern at the node level for each group, along with a comparison of their whole-brain distributions illustrated on the right, with each point representing a brain region (90 brain regions for each group). Pairwise comparisons of these distributions were performed using two-sample *t*-tests, with *P*-values FDR-corrected for multiple comparisons using the Benjamini–Hochberg method (*$P < 0.05$; **$P < 0.01$; ***$P < 0.001$). Box plots, overlaid on data points, depict the interquartile range (IQR) and the median value of the distribution. Whiskers extend to the nearest points ±1.5× IQR above and below the 25th and 75th percentiles.

understanding of how functional specialization emerges and how early developmental risk alters these trajectories.

Results

The overlapping structure of neonate cerebral cortex

Representative functional communities identified from term-born infants are illustrated in Fig. 1a. We found that connections within the same network exhibited a high degree of similarity, with the strongest within-system similarity found in sensorimotor, subcortical, and visual networks (Fig. 1b, c). Interestingly, the visual system appeared to be divided into two distinct components, corresponding to the primary and secondary visual cortex (V1 and V2), while a similar subdivision was observed in the default-mode network (DMN). Connections between SMN/VAN/SUB, as well as those between DAN/FPN/DMN, exhibited high levels of between-system similarity (Fig. 1c). Notably, within-system edge similarity significantly differed across functional systems (ANOVA; $F_{529} = 22.74$, $P < 10^{-15}$; Fig. 1d). To further characterize the overlapping community structure at the regional level, we calculate, for each node, the fraction of its edges belonging to each edge community. This approach enables us to intuitively describe edge communities in terms of their correspondence to canonical functional systems (Fig. 1e). By mapping these regional affiliations onto anatomical brain surfaces (Fig. 1f), we can visualize the topography of edge communities in a biologically meaningful way. For example, regions within the SMN are simultaneously involved in edges assigned to communities 1, 2, 5 and 6, thereby connecting brain regions across multiple other systems, similar to previous findings in adults[28].

Edge PC patterns of neonates

Edge participation coefficient exhibited consistently high values for within-system connections, with the highest values observed in the VIS, SMN (Fig. 2a). Moreover, edge PC patterns differed significantly across the three groups (two-sample *t*-test; PT1 vs. PT2: $T_{8008} = 53.49$, $P < 10^{-15}$; PT1 vs. FT: $T_{8008} = 79.35$, $P < 10^{-15}$; PT2 vs. FT: $T_{8008} = 24.23$, $P < 10^{-15}$, FDR-corrected using the Benjamini–Hochberg method). At the nodal level (Fig. 2b), these group differences remained significant (two-sample *t*-test; PT1 vs. PT2: $T_{178} = 22.02$, $P < 10^{-15}$; PT1 vs. FT: $T_{178} = 33.90$, $P < 10^{-15}$; PT2 vs. FT: $T_{178} = 11.63$, $P < 10^{-15}$, FDR-corrected using the Benjamini–Hochberg method). However, the normalized entropy showed no significant group differences in whole-brain distributions between the PT1 and PT2 groups. The nodal participation coefficient showed no significant group difference in whole-brain distributions between the PT2 and FT groups (Supplementary Fig. 3a, b). These findings remained consistent when restricting the analysis to preterm infants who underwent scans at both timepoints in the PT1 and PT2 groups (Supplementary Fig. 4). Additionally, region-level statistical comparisons across the three groups revealed that edge PC exhibited more widespread and pronounced group differences across the whole brain compared to the normalized entropy and nodal participation coefficient (Supplementary Fig. 5).

Effect of postmenstrual age at scan

When examining the correlation with PMA at scan, numerous connections exhibited significant growth in the full-term group, fewer in preterm infants at TEA, and almost none in preterm infants at birth (Fig. 3a). Specifically, full-term neonates showed greater growth in connections between the VIS and other systems, as well as between the LIM, FPN, and DMN. In contrast, preterm infants at TEA exhibited more growth in within-system connections of the VIS, SMN, and DMN, along with between-system connections involving the DMN (Fig. 3b). A comparison of growth effects within the full-term group across the three measures—the normalized entropy, nodal PC, and the proposed edge PC—is presented in Supplementary Figs. 6 and 7. Only three brain regions exhibited significant age-related entropy changes without correction, and none survived Bonferroni correction ($P < 0.01$). For nodal PC derived from nodal FC, some regions within the VIS, LIM, and VAN showed significant growth and remained significant after Bonferroni correction ($P < 0.01$). In contrast, nearly all brain regions demonstrated significant growth in edge PC, even after Bonferroni correction ($P < 0.01$).

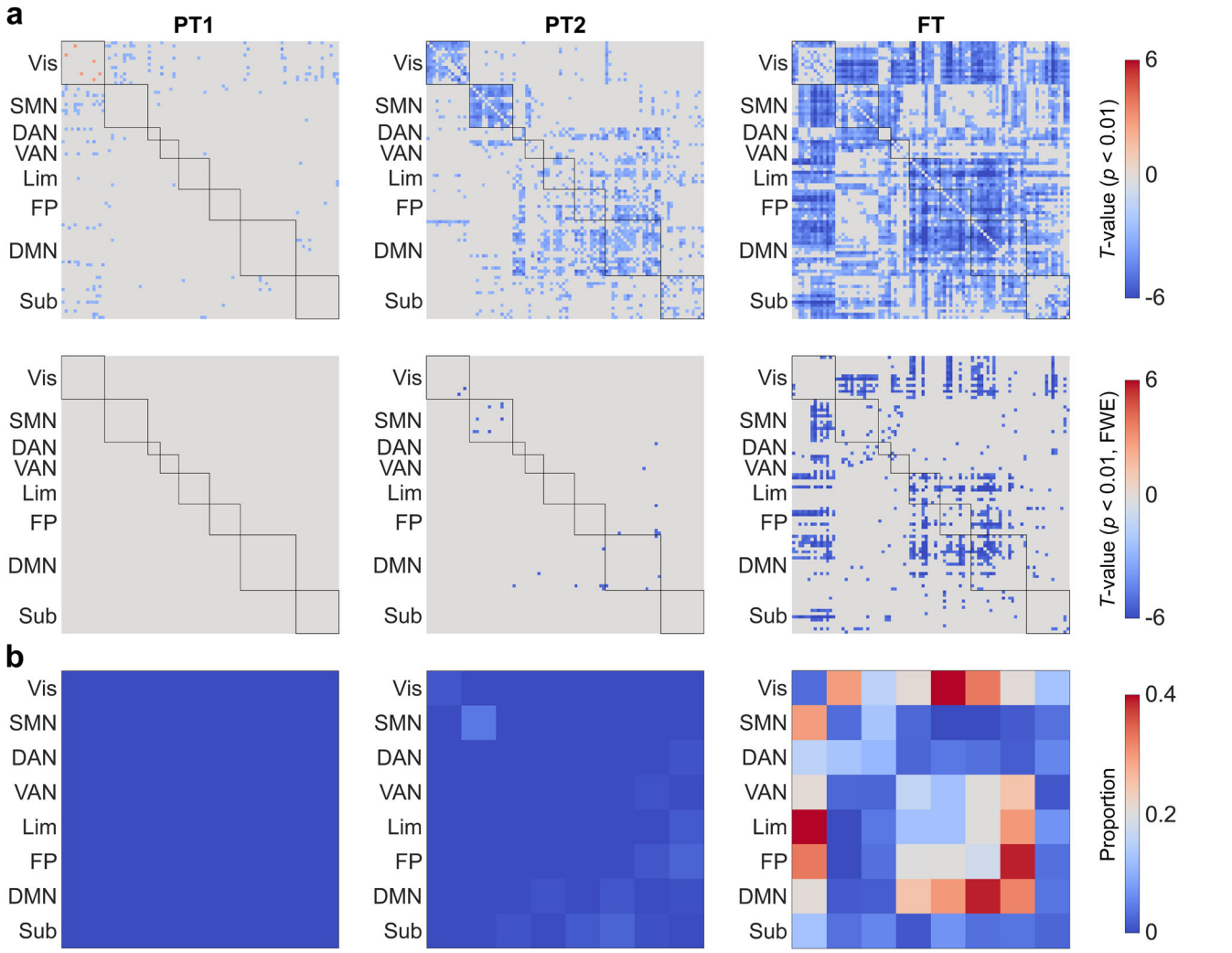

Fig. 3 | Edge-wise PMA effect on edge PC. a The growth patterns of edge PC at the connectional level with the significance thresholded at uncorrected *P*-value < 0.01 (upper row) and Bonferroni-corrected *P*-value < 0.01(lower row) within each of the three groups (PT1: $n = 152$, PT2: $n = 135$, FT: $n = 494$). For visualization, the node-by-node matrices were reordered according to their affiliated systems. **b** The proportion of edges with significant growth for each system based on the thresholding of Bonferroni-corrected *P*-value < 0.01 for each group.

Developmental fluctuations of edge PC

The dynamic development fluctuations of edge PC for both preterm and full-term groups, analyzed using a sliding window approach along PMA at scan, are illustrated in Fig. 4a, b. In addition, the linear relationships between PMA at scan and edge PC for both within- and between-network connections are presented in Supplementary Figs. 8, 9, and 10. A consistent overall decreasing trend in edge PC was observed across all networks and connection types, with within-network edge PC consistently higher than between-network edge PC (Fig. 4c). This pattern was particularly pronounced in the VIS, SMN, DAN, VAN, and SUB for all groups. However, the DMN was the only network where no significant difference was observed between within- and between-network edge PC in both the FT and PT2 groups.

Association between edge PC and follow-up cognitive outcomes

The brain-behavior relationship between edge PC and cognitive outcomes at 18-month age was examined and is shown in Fig. 5. Specifically, for the connections that exhibited significant growth within full-term neonates (Fig. 3b), two prominent types were identified: (1) VIS-associated between-system connections and (2) within-system connections involving the LIM, FPN, and DMN modules. These networks are also widely implicated in early cognitive functions and neurodevelopmental outcomes[34]. When correlating the averaged edge PC of these connection sets with DSID-III scores at 18 months, significant negative correlations were observed for the language domain ($P < 0.05$, FDR-corrected using the Benjamini–Hochberg method).

Transcriptomic and cellular architectures of edge PC development

To explore the transcriptomic basis of edge PC development, we utilized the BrainSpan Atlas[35,36] to obtain spatial transcriptomic profiles of 22494 genes across 14 brain regions. We linked edge PC development (Fig. 6a) with gene co-expression amplitudes (Fig. 6b) by employing Pearson's correlation. Permutation testing identified 1518 genes significantly correlated with edge-wise *T*-values ($P_{perm} < 0.001$), which were subsequently ranked in descending order according to their correlation coefficients. The genes with the highest positive and negative correlations are highlighted in Fig. 6c.

GO enrichment analysis revealed that genes associated with edge PC development were significantly enriched in neurodevelopmental processes, cellular signaling, and structural organization (Fig. 6d). Key biological processes included vasculature development, neuron projection development, enzyme-linked receptor protein signaling, and endothelium development, while molecular functions were enriched for transcription factor binding, kinase activity, and guanyl nucleotide binding, indicating roles in

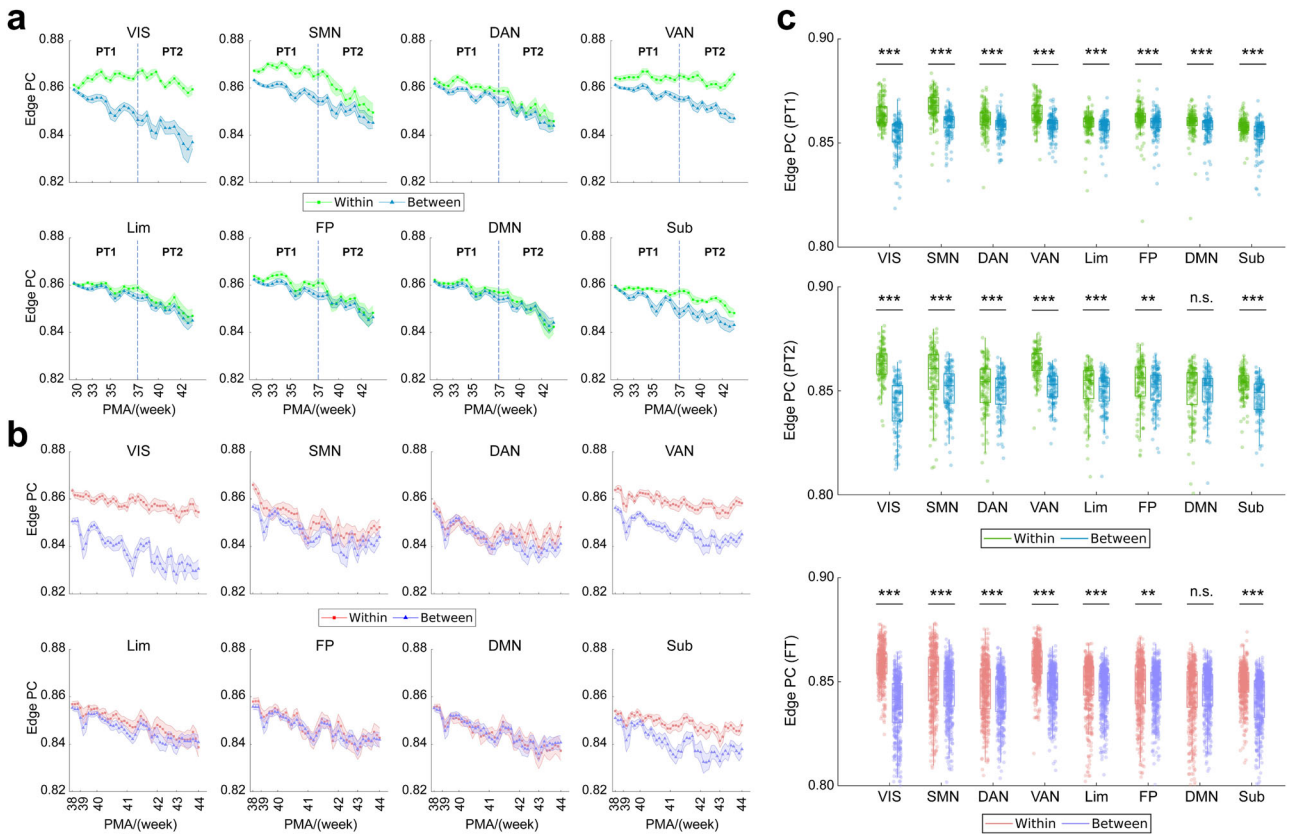

Fig. 4 | Dynamic development of edge PC at the system level. a Dynamic fluctuations of edge PC at within- and between-system level for preterm infants. For each subgroup of 20 infants generated using the sliding window approach, the mean (dots) and standard error (shaded area) of edge PC values were calculated separately for within-system and between-system connections. Within-system edge PC refers to connections linking two nodes within the same functional system, while between-system edge PC refers to connections linking nodes from different systems. **b** Dynamic fluctuations of edge PC at within- and between-system level for full-term infants. **c** Comparisons of within- and between-system edge PC across all eight functional systems. Paired *t*-tests were performed for each group, with each point representing an individual infant (PT1: $n = 152$, PT2: $n = 135$, FT: $n = 494$). Box plots, overlaid on data points, depict the interquartile range (IQR) and the median value of the distribution. Whiskers extend to the nearest points ±1.5× IQR above and below the 25th and 75th percentiles. Statistical details are provided in Supplementary Table 1 (* $P < 0.05$; ** $P < 0.01$; *** $P < 0.001$, FDR-corrected using the Benjamini–Hochberg method).

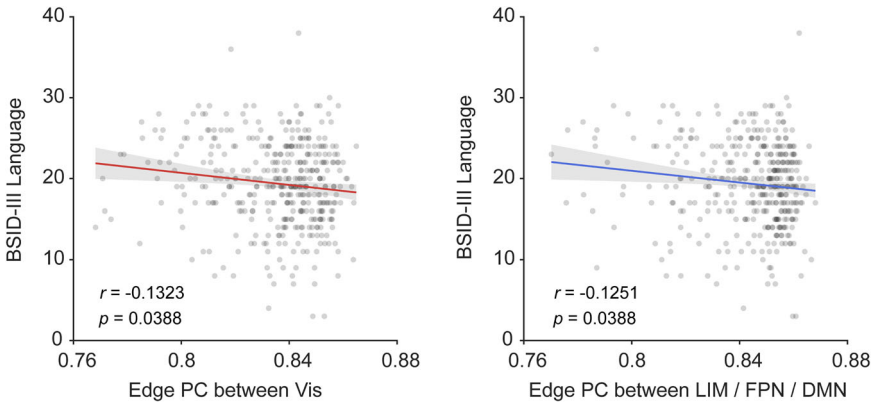

Fig. 5 | Association between edge PC and the BSID-III scores at 18 months of age. Significant negative correlations were observed for connections between Vis and other systems ($n = 394$, $r = -0.1323$, CI = [−0.2281, −0.0339], $P = 0.0388$), and between LIM/FPN/DMN ($n = 394$, $r = -0.1251$, CI = [−0.2212, −0.0266], $P = 0.0388$). *P*-values were FDR-corrected for multiple comparisons using the Benjamini–Hochberg method. Full behavioral correlation results are provided in Supplementary Table 2, and results for additional BSID-III subscales are shown in Supplementary Fig. 11.

gene regulation and intracellular signaling. Cellular components highlighted enrichment in axon, microtubule, glutamatergic synapse, and cell-substrate junction, suggesting involvement in neuronal structure and synaptic organization. Clustering of significant GO terms (Fig. 6f and Supplementary Fig. 12) further emphasized pathways related to glial differentiation, small GTPase-mediated signaling, head development and autophagy regulation, reinforcing the link between transcriptional profiles and early brain development. Additionally, cell type-specific analysis demonstrated that these genes were predominantly expressed in endothelial cells (number = 136, adjusted $P_{perm} < 0.001$), excitatory neurons (number = 110, adjusted $P_{perm} = 0.012$), and astrocytes (number = 102, adjusted $P_{perm} = 0.012$) (Fig. 6e).

To further elucidate the biological pathways underlying edge PC development, we performed GSEA on the ranked gene list (Fig. 6g). The results revealed significant enrichment in typical neurodevelopmental and metabolic pathways. Specifically, positive enrichment was observed in

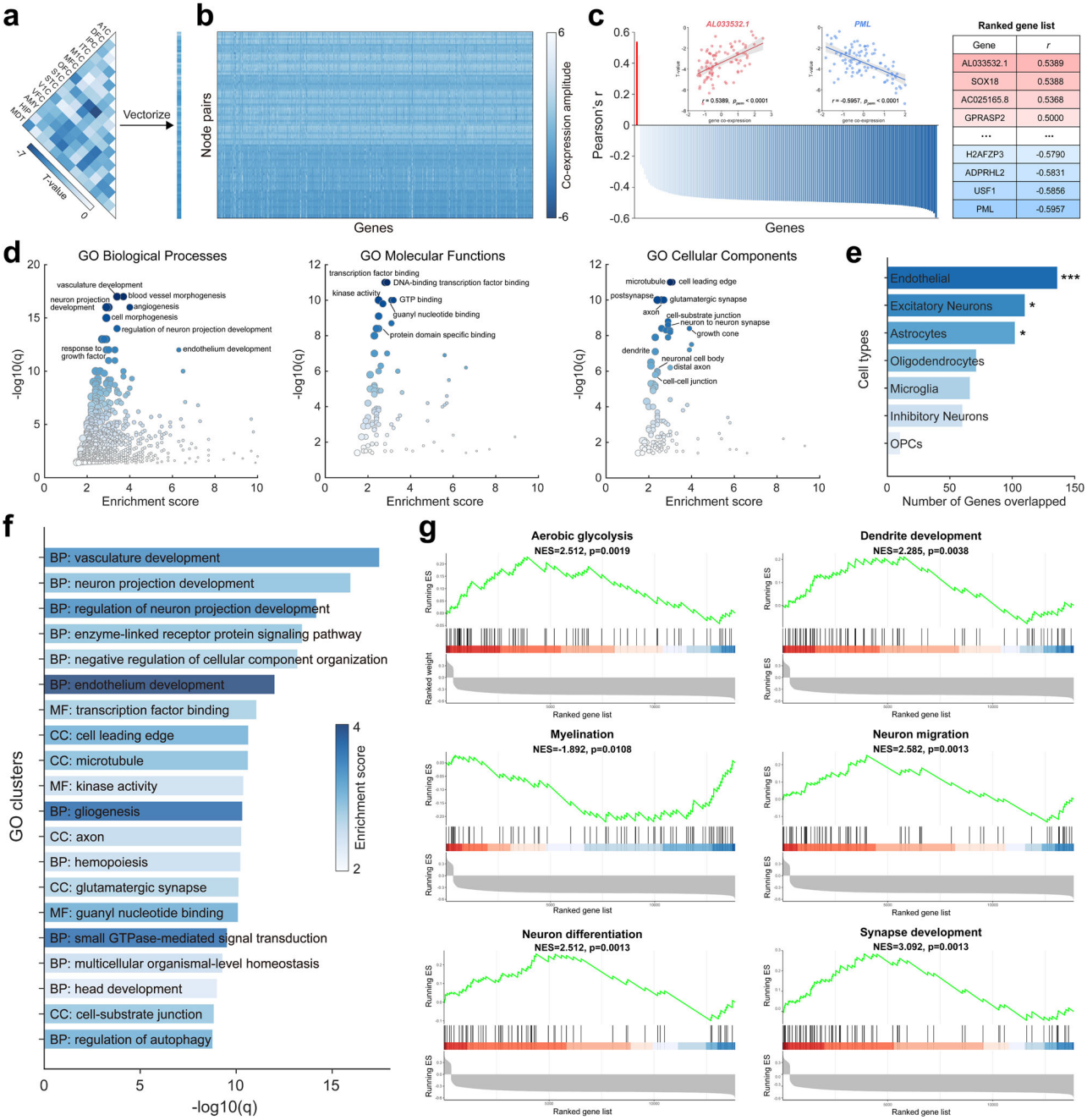

Fig. 6 | Association between edge PC development and transcriptomic profiles. **a** Edge-wise *T*-values represented in matrix form. **b** Normalized gene co-expression profiles, comprising 22494 genes across paired brain regions. **c** The ranked list of 1518 genes significantly correlated with edge-wise *T*-values. **d** Gene Ontology (GO) enrichment analysis of selected genes for three ontology categories: Biological Processes (BP), Molecular Functions (MF), and Cellular Components (CC). Note that the *q*-value represents the FDR-corrected *P*-value using the Benjamini–Hochberg method. **e** The number of selected genes overlapping with cell type-specific gene sets (* $P < 0.05$; ** $P < 0.01$; *** $P < 0.001$, FDR-corrected using the Benjamini–Hochberg method). **f** Top 20 enriched GO clusters across selected gene list, color-coded by enrichment scores, which are detailed in Supplementary Table 6. **g** Gene set enrichment analysis (GSEA) highlights typical neurodevelopmental processes and neuronal metabolic pathways significantly enriched at the top or bottom of the ranked gene list. The statistical significance of the enrichment score (ES) was assessed using permutation tests by randomly shuffling the phenotype labels 10,000 times. The normalized enrichment score (NES) was computed by dividing the observed ES by the mean ES from the permutation distribution.

pathways related to aerobic glycolysis ($NES = 2.512$, $P_{perm} = 0.0019$), dendrite development ($NES = 2.285$, $P_{perm} = 0.0038$), neuron migration ($NES = 2.582$, $P_{perm} = 0.0013$), neuron differentiation ($NES = 2.512$, $P_{perm} = 0.0013$), and synapse development ($NES = 3.092$, $P_{perm} = 0.0013$), indicating their potential roles in shaping edge-wise functional organization. In contrast, myelination ($NES = -1.892$, $P_{perm} = 0.0108$) was negatively enriched, reflecting a distinct molecular pattern. These findings highlight the transcriptional underpinnings of neural connectivity, emphasizing processes related to neuronal maturation, synaptic function, and metabolic regulation.

Discussion

In this work, we introduced the edge-centric participation coefficient (ePC), a metric quantifying the connectional modular flexibility and functional integration, to examine the dynamic evolution of the brain's functional connectome during infancy. Notably, the edge-centric approach provides

complementary insights relative to traditional node-based measures, as demonstrated by the broader spatial extent and heightened sensitivity observed in our analyses. Our study revealed three pivotal findings: (1) Preterm infants exhibited significantly higher edge PC compared to term-born peers, indicating delayed functional network specialization during critical developmental windows; (2) Edge PC of connections exhibiting substantial growth effects during infancy—particularly those involving the visual and high-order networks—are negatively correlated with 18-month cognitive scores, suggesting that refined functional specialization may contribute to more favorable cognitive outcomes; (3) Transcriptomic analyses identified genes involved in neurodevelopmental, vascular, and metabolic processes, linking activity-dependent plasticity and neuronal maturation to functional network refinement. By establishing edge PC as a sensitive biomarker of preterm-term divergence, our work provides a mechanistic blueprint for optimizing the timing of neurodevelopmental interventions, with direct implications for mitigating cognitive deficits in high-risk infants. These findings redefine connectome maturation as an edge-resolved process, where individual connections act as both indicators and architects of emergent cognitive capacities—a paradigm shift with profound implications for understanding neurodevelopmental disorders.

Our findings demonstrate that ePC not only reveals more robust and widespread group-level differences across the brain but also exhibits greater sensitivity to age-related developmental changes. Compared with traditional measures such as nodal participation coefficient and normalized entropy, the edge-centric approach offers complementary and finer-grained insights into the evolving architecture of the infant connectome. These results align with growing evidence that edge-centric models provide unique insights into dynamic network reconfiguration and are particularly sensitive to individual idiosyncrasies in brain organization[28–33].

Our study marks a significant advancement in developmental neuroscience by introducing an edge-centric approach to analyzing the functional connectome during infancy. This methodological shift is not merely a technical refinement but a fundamental rethinking of how we perceive and analyze neural connectivity. Traditionally, neuroimaging studies have been dominated by node-based analyses, which focus on the roles of specific brain regions. Our approach, however, examines the dynamic interactions between edges, offering a more nuanced and intricate perspective on the connectome's evolution[3,37]. The pronounced fluctuations in edge PC observed in our study align with emerging theories highlighting the importance of network reconfiguration and synaptic plasticity in early brain development[38].

One of the most striking findings of our research is the differential trajectory of connectome development we observed between preterm and full-term infants. For preterm-born infants scanned at birth, edge PC most correlated with PMA at scan were related to the between-network connections, such as those linking the sensorimotor and visual systems, the ventral attention and visual systems, and "higher-order" networks with the subcortical network. In contrast, for preterm infants scanned at TEA, edge PC values showed weaker or no correlation with PMA at scan, except for edges within the visual, sensorimotor and subcortical networks, as well as connections between "higher-order" networks. When looking at term-born infants, edge PC values of multiple edges were highly correlated with PMA at scan, particularly those linking the visual to other networks, and between "higher-order" networks. Notably, these correlations were negative, indicating a refinement process in which functional networks become more specialized as the brain develops.

These distinctions underscore the profound impact of birth timing on neural development, a topic of increasing interest in pediatric neuroimaging[39,40]. The alterations in edge PC observed in preterm infants might reflect deviations from the typical trajectory of synaptic development and pruning, potentially contributing to the cognitive and behavioral differences frequently reported in this population[41,42]. Our study provides a nuanced understanding of how early environmental and biological factors critically shape the foundational architecture of the brain's network, potentially setting a trajectory that diverges from normal development.

Our analysis of edge PC across the developing brain has shed light on the highly dynamic and adaptable nature of infant brain networks. Interestingly, in preterm-born infants scanned before reaching TEA, edge PC values of certain edges—primarily within the visual and sensorimotor systems—exhibited a positive correlation with PMA at scan. Conversely, edges connecting the visual system with the dorsal and ventral attention systems exhibited a negative correlation with PMA at scan, though none of these edges survived FWE correction. As the preterm brain continued to develop, a growing number of within-network edge PC values became associated with maturation, particularly within the visual, sensorimotor, and "higher-order" networks, such as the DMN and FPN. In term-born infants, edges connecting the visual system with other networks, as well as those linking "higher-order" networks, demonstrated robust associations with normal brain maturation.

The observed variability in these patterns likely mirrors key biological processes, such as synaptic density fluctuations and the formation of critical neural pathways[43–46]. These results reinforce the notion that brain development during infancy is a highly individualized process, influenced by a myriad of factors including genetic predisposition, environmental exposures, and early life experiences[47,48]. Understanding these dynamic patterns is crucial for unraveling the complex mechanisms underlying both typical and atypical brain development. Our results provide valuable insights into the early development of the neonatal cerebral cortex. Specifically, a subset of connections emerges at the late stage of gestation and continues to develop after birth, during which several within-network connections begin to specialize in preterm infants. In full-term infants, however, multiple connections across the entire cortex become relatively robust and specialized as the brain matures, reflecting a trajectory of more structured neuronal network organization.

The observed negative correlation between edge PC in visual and high-order networks and 18-month language scores in full-term infants suggests that greater modular specialization—reflected by lower edge PC—is associated with more favorable cognitive development. This finding aligns with previous work demonstrating that early functional network segregation supports the emergence of higher-order cognitive functions during infancy and early childhood[23,49–53]. In full-term populations, more modular and efficiently organized networks, particularly in visual, default-mode and frontoparietal networks, have been linked to improved language outcomes[54,55]. Our results suggest that edge-level measures of functional integration and segregation may capture meaningful individual variability in early cognitive trajectories, even within normative development. These findings highlight edge PC as a promising marker of functional connectome maturation during the first year of life.

Although early ePC values were significantly associated with 18-month cognitive outcomes in full-term infants, no such relationships were observed in the preterm cohorts (PT1 or PT2), as reported in Supplementary Tables 3 and 4. These findings suggest that the developmental relevance of early edge-level network organization may differ in preterm infants, possibly due to additional clinical, environmental, or maturational factors that influence later outcomes[56–58]. Future studies with larger samples and richer clinical phenotyping will be needed to clarify the predictive value of edge-centric network measures in high-risk populations[59,60].

Our findings demonstrate a strong transcriptional association between edge PC development and genes involved in neurodevelopmental, vascular, and metabolic processes. GO analyses showed enrichment in neuron projection development, synapse organization, and vascular maturation, highlighting the interplay between neuronal and neurovascular factors in shaping functional connectivity. The formation and maintenance of the central nervous system (CNS) vasculature are crucial for a properly functioning brain[61,62], relying on vasculogenesis and sprouting angiogenesis during both embryonic and postnatal development, driven by various pro- and anti-angiogenic factors[63]. Cell type-specific analysis highlighted the predominant expression of these genes in endothelial cells, excitatory neurons, and astrocytes, underscoring their roles in both neuroprotection and neurodevelopment. Physiologically, endothelial cells and astrocytes

constitute the structural foundation of the blood–brain barrier (BBB) for lining the cerebral blood vessels and interacting with various types of CNS cells to maintain neural homeostasis[64,65]. The BBB, which has been shown to be functional as early as 8 weeks of gestation, plays a critical role in protecting the developing fetal brain and maintaining an optimal environment for neurodevelopment[66]. GSEA results further emphasize the contribution of neuronal metabolic pathways and neurodevelopmental processes to early postnatal development of the brain. The infancy marks a period of rapid brain growth, characterized by glial proliferation, axonal formation, and dendritic arborization, leading to dramatic increases in brain volume and cortical surface areas, while synaptic pruning acts to regulate these processes[67,68]. Concurrently, myelination increases white matter volume and the maturation of microstructural integrity along neural tracts[68,69]. These neurodevelopmental processes, including synaptogenesis, pruning, synaptic remodeling, and myelination, are foundational to the establishment of neural circuits[70]. Collectively, our findings provide a transcriptional framework for understanding the potential molecular mechanisms underlying the functional network development of the early brain, enhancing insights into how genetic regulation shapes neuronal connectivity, synaptic architecture, and cerebrovascular interactions during early brain maturation.

One overarching limitation of this study concerns the interpretability of eFC. While traditional nFC is widely accepted and often interpreted as a proxy for interregional communication[71], eFC remains a relatively novel and high-dimensional framework[30]. Its interpretability is inherently more complex, as it captures co-fluctuations between pairs of edges rather than between brain regions directly. Although this study introduces the edge participation coefficient (ePC) as a summary measure to quantify the functional diversity of eFC at the connectional level, the biological meaning of edge-centric representations remains an open question. Future work is needed to better elucidate the neurophysiological underpinnings of eFC, explore its low-dimensional representations, and clarify how edge-wise metrics relate to known patterns of structural connectivity, neural synchrony, and behavioral outcomes across development.

A second limitation lies in the strategy used to estimate edge communities. In this study, we employed the *k*-means algorithm to partition edge-wise co-fluctuation time series into a fixed number of clusters based on their similarity. This choice was primarily motivated by computational efficiency, as k-means proved significantly faster than alternative methods such as modularity maximization[72] or Infomap[73]. However, a wide range of alternative algorithms could, in principle, be applied to edge time series or eFC for community detection—including graph-based clustering methods[74], as well as time-series decomposition techniques like independent component analysis (ICA)[75], which has been particularly effective in neuroimaging applications[76]. Applying these approaches to eFC data, however, is computationally challenging due to the high dimensionality and the need to process large, fully weighted, and signed matrices[30]. Future work should explore the impact of different clustering strategies on the resulting edge community structure and investigate scalable solutions that reduce the computational demands associated with edge-level community detection.

Yet another limitation is the potential influence of medical comorbidities—such as intraventricular hemorrhage, bronchopulmonary dysplasia, and sepsis—on brain development in preterm infants[77,78], which we did not explicitly control for in our primary analyses. Additionally, not all preterm infants underwent MRI at both early postnatal and term-equivalent age (TEA) timepoints; to maximize sample size and minimize bias from mortality, clinical contraindications, or loss to follow-up, we conducted cross-sectional analyses at each timepoint. To address this limitation, we performed a sensitivity analysis restricted to infants with longitudinal scans and applied a linear mixed-effects (LME) model controlling for gestational age at birth, sex, birth weight, and head motion. These additional analyses (reported in Supplementary Figs. 4 and 5) confirmed the robustness of our main findings. Nonetheless, future studies incorporating detailed clinical data and prospective longitudinal designs will be essential to disentangle the specific effects of prematurity, disease burden, and scan availability on neurodevelopment[79,80].

Table 1 | Demographic and cognitive characteristics of the study cohort

	Group		
Characteristic	**PT1 (*n* = 152)**	**PT2 (*n* = 135)**	**FT (*n* = 494)**
Female (%)	70 (46)	60 (44)	219 (44)
GA at birth, mean (SD), weeks	31.41 (3.55)	31.79 (3.75)	40.07 (1.17)
PMA at scan, mean (SD), weeks	33.86 (2.35)	40.95 (2.05)	41.40 (1.64)
BSID-III follow-up	117 (76.97%)	100 (74.07%)	394 (79.76%)
Cognition, mean (SD)	9.67 (2.54)	9.82 (2.60)	10.20 (2.18)
Language, mean (SD)	18.41 (6.21)	19.07 (6.08)	19.39 (5.28)
Motor, mean (SD)	19.76 (3.66)	19.56 (3.76)	20.67 (3.20)

GA gestational age, *PMA* postmenstrual age, *SD* standard deviation, *FT* Full-term infants.
PT1: preterm infants scanned at birth; PT2: preterm infants scanned at term-equivalent age.

Methods

Participants

All participants in this study were recruited as part of the developing Human Connectome Project (dHCP, http://www.developingconnectome.org/)[81], approved by the UK National Research Ethics Authority. Written consent was obtained from all participating families prior to imaging. All ethical regulations relevant to human research participants were followed. Term-born infants were recruited from the postnatal wards and were considered eligible if they were medically stable with no clinical concerns. Preterm-born infants were recruited from the neonatal unit and postnatal wards. Exclusion criteria included a history of severe compromise at birth requiring prolonged resuscitation, a diagnosed chromosomal abnormality, any treatment for clinically significant brain injury, and any contraindication to MRI scanning. We selected 781 structural-functional datasets from the 2021 (third) dHCP data release, including term-born neonates scanned from 37 to 44.5 weeks postmenstrual age (PMA; FT group), preterm-born neonates scanned at birth (PT1 group) and preterm-born neonates scanned at term-equivalent age (TEA; PT2 group). The Bayley III Scales of Infant and Toddler Development (BSID-III)[82] collected at 18 months corrected age were available for a subset of infants. Detailed information is listed in Table 1.

MRI acquisition

All scans were collected in the Evelina Newborn Imaging Center, Evelina London Children's Hospital, using a 3T Philips Achieva system. All infants were scanned during natural sleep without sedation in a scanner environment optimized for safe and comfortable neonatal imaging, including a dedicated transport system, positioning device and a customized 32-channel receive coil, with a custom-made acoustic hood[83]. All scans were supervised by a pediatrician or neonatal nurse experienced in MRI procedures; vital signs, including oximetry, temperature and heart rate were monitored throughout data acquisition.

High-resolution T1- and T2-weighted anatomical multi-slice fast spin-echo images were acquired with in-plane resolution $0.8 \times 0.8\ mm^2$ and 1.6 mm slices overlapped by 0.8 mm. Fifteen minutes of high temporal resolution resting-state functional MRI (rs-fMRI) optimized for neonates was acquired using a multi-slice gradient-echo echo planar imaging (EPI) sequence with multiband excitation (repetition time = 392 ms, echo time = 38 ms, flip angle = 34°, multiband factor = 9, 2.15 mm isotropic, 2300 volumes).

Functional data preprocessing

The rs-fMRI data were preprocessed using the dHCP pipeline and an in-house pipeline optimized for neonatal imaging[84], including susceptibility dynamic distortion together with intra- and inter-volume motion correction for each participant. To regress out artefacts related to head motion, cardiorespiratory and multiband acquisition, 24 extended rigid-body

motion parameters, as well as single-subject independent component analysis (ICA) noise components identified using the FMRIB Software Library (FSL, https://fsl.fmrib.ox.ac.uk/fsl/fslwiki/)[85] were regressed out. Denoised images were subsequently registered into native T2 space and then nonlinearly registered to the dHCP age-specific template and finally to the UNC Infant Brain Atlas of Neonates[86], using the advanced normalization tools (ANTs, https://github.com/ANTsX/ANTs)[87]. This dedicated infant atlas was used to define 90 parcels on the cerebral cortex, which are also mapped to Yeo's 7 canonical functional networks[88] (VIS, visual; SMN, sensorimotor network; DAN, dorsal attention network; VAN, ventral attention network; LIM, limbic; FPN, frontoparietal network; DMN, default-mode network) together with the subcortical network (SUB).

While the functional MRI preprocessing pipeline for the dHCP addresses the potential problem of head motion in rs-fMRI data, motion is also a surrogate marker of the arousal state of the infant, which interacts with the underlying neural activity[89]. To address this issue, we excluded participants with DVARS (the root mean square intensity difference between successive volumes) >1.5 interquartile range (IQR) above the 75th centile in more than 230 (10%) of the 2300 volumes. A bandpass temporal filtering at 0.01–0.1Hz together with a global signal regression was then performed using AFNI[90]. Following these preprocessing steps, the voxel-wise fMRI time series were averaged into their corresponding parcels of the atlas and then z-scored.

Edge functional network construction

For the functional connectome, temporal statistical dependencies between activity time courses of brain regions are estimated from fMRI to define functional connectivity (FC) that can be modeled and analyzed using network science. The most common measure of this dependence is calculated as the Pearson correlation coefficient between every pair of nodal time series. This procedure results in a node-by-node similarity matrix referred to as an estimate of functional connectivity. While a novel modeling framework[28] has been recently proposed to investigate functional brain network data from an edge-centric perspective by slightly modifying the Pearson correlation measure. Briefly, an edge time series encoding the moment-by-moment co-fluctuations magnitude between parcels i and j is generated by calculating the element-wise product of two z-scored node time series, z_i and z_j. Notably, the mean of an edge time series equals the Pearson correlation of the corresponding two nodal time series. Repeating this operation for every pair of parcels results in a set of edge time series, each of length T. Let $c_{ij} = [z_i(1) \cdot z_j(1), \cdots, z_i(T) \cdot z_j(T)]$ and $c_{uv} = [z_u(1) \cdot z_v(1), \cdots, z_u(T) \cdot z_v(T)]$ be the time series of edges $\{i, j\}$ and $\{u, v\}$, respectively. Edge functional connectivity (eFC) can be calculated as:

$$eFC_{ij,uv} = \frac{\sum_t c_{ij}(t) \cdot c_{uv}(t)}{\sqrt{\sum_t c_{ij}(t)^2}\sqrt{\sum_t c_{uv}(t)^2}} \quad (1)$$

Clustering algorithm

Here, we used a standard k-means algorithm with Euclidean distance to directly cluster edge time series. The choice to use k-means algorithm was practically motivated, as k-means exhibited significantly faster runtimes than other algorithms—for example, modularity maximization[72] and Infomap[73], which have been widely used to detect communities in functional brain networks. To establish a group-level reference, we first concatenated edge time series across all term-born infants and applied k-means clustering to derive representative community centroids. These centroids were then used to initialize subject-specific clustering to ensure cross-subject consistency in edge community assignments. The number of clusters was varied from $k = 2$ to $k = 20$. The clustering algorithm was run for 1000 iterations, thus providing a community affiliation for each edge at each k.

To determine the number of clusters (k), we explored a range from $k = 2$ to 20 and repeated the clustering 1000 times per k value to ensure robustness. We selected $k = 10$ as a representative resolution based on both methodological precedent[28,30] and empirical evidence: as shown in Supplementary Figs. 1 and 2, the normalized entropy maps and edge participation coefficient patterns remain highly consistent across a wide range of k-values, indicating that our core findings do not depend on a specific choice of k. This consistency aligns with previous studies in adult populations[28,30], further supporting the robustness of our clustering solution.

Community overlapping measures

The output of the clustering algorithm is a partition of edges into non-overlapping clusters. Every edge $\{i, j\}$ was assigned to one of the k clusters. There were N-1 edges related to each brain region (self-connections excluded). The affiliation of region i to edge cluster c is defined as:

$$\alpha_{ic} = \frac{1}{N-1}\sum_{i \neq j} \delta(c_{ij}, c) \quad (2)$$

Where $c_{ij} \in \{1, \cdots, k\}$ was the community assignment of edge $\{i, j\}$, and $\delta(x, y)$ is the Kronecker delta, whose value is 1 if $x = y$ and 0 otherwise. By treating the vector $\alpha_i = [\alpha_{i1}, \cdots, \alpha_{ik}]$ as a probability distribution, we can calculate the entropy of this distribution as:

$$e_i = -\sum_c \alpha_{ic} \log_2 \alpha_{ic} \quad (3)$$

For normalization, this measure was divided by $\log_2 k$ so that it was bounded to the interval [0, 1]. The normalized entropy measures the extent to which region i's community affiliations are distributed evenly across all communities (normalized entropy is close to 1 and high overlap) or concentrated within a small number of communities (normalized entropy is close to 0 and low overlap).

Edge community similarity

Each edge was assigned to a single community after the clustering algorithm. We can rearrange these edge communities into the triangle of an $N \times N$ matrix, C, whose element c_{ij} denotes the community assignment of the edge connecting nodes i and j. The ith column of C, $c_i = [c_{1i}, \cdots, c_{Ni}]$, encodes the community affiliations of all edges related to node i. Note that the element c_{ii} is empty with self-connections excluded. In order to compare the edge communities of nodes i and j, we can measure the similarity of vectors c_i and c_j as the fraction of elements in both vectors with the same community label. It is possible to compare the edge communities of nodes i and j by measuring the similarity of vectors c_i and c_j as the fraction of elements in both vectors with the same community label. That is:

$$s_{ij} = \frac{1}{N-2}\sum_{u \neq i,j} \delta\left(c_{ui}, c_{uj}\right) \quad (4)$$

Note the normalization of over N-2 because the self-connections c_{ii} and c_{jj} are ignored. Calculating this similarity for all pairs of nodes generates the similarity matrix $S = \{s_{ij}\}$.

Edge participation coefficient

Node-centric network can be partitioned into communities of nodes, also referred to as modules. Some nodes have connections that are distributed across multiple modules, whereas others are only connected with other nodes in their own module. The participation coefficient (PC) that provides insight into how specific nodes communicate between modules is typically used to measure this attribute in network neuroscience. Similarly, we can calculate the participation coefficient of a given node in the modular eFC network to explore the functional role of each edge from the perspective of interacting edges.

Participation coefficient measures the extent to which a node's connections in the eFC network are distributed across edge communities uniformly or not. The closer the value is to 1, the more uniformly a given node in the eFC network interacts with all edge communities. Formally, the PC of

node i is given by:

$$PC_i = 1 - \sum \left(\frac{k_i(m)}{k_i} \right)^2 \quad (5)$$

Here, $k_i(m)$ is the strength of node i to all nodes in community m, and k_i is the total strength of node i. The edge PC was calculated for each edge, across all subjects, using the previously defined term-born representative community labels. For comparison, we also calculated the nodal PC based on the conventional FC matrix and the systems communities of brain regions and the normalized entropy based on the detected edge communities. All participation coefficient measures are computed using the Brain Connectivity Toolbox (https://sites.google.com/site/bctnet/).

While broader edge-centric frameworks—such as edge functional connectivity and edge community structure—have been explored in recent works[28–31], our implementation of the ePC metric represents an extension of these approaches to characterize the modular integration properties of individual connections. This provides a complementary perspective to node-based measures, offering additional insight into the functional roles of specific connections during early brain development.

Transcriptomic association analysis

To explore the potential molecular mechanisms underlying functional changes as the brain develops, we utilized the BrainSpan Atlas[35,36], a developmental gene expression dataset, to examine the transcriptomic associations of edge PC development. This Atlas provides transcriptomic data of 52376 genes across 524 brain samples from 42 individuals, spanning from eight post-conceptional weeks to 40 postnatal years. In this study, to match the postmenstrual age of the full-term cohort included in our developmental transcriptomic analysis, we specifically analyzed data from a donor aged 37 postmenstrual weeks. For this donor, gene expression data were available for only 14 cortical regions, as two regions lacked sufficient expression data (further details on these regions are provided in Supplementary Table 5). After excluding genes with missing values in any region, a total of 22494 genes were retained for further analysis.

We calculated edge PC values between all pairs of the 14 brain regions using the previously documented approach. For each dependent variable (edge PC between any two regions), we applied a general linear model (GLM) with PMA at scan as the independent variable, and GA at birth, sex, birth weight and head motion as covariates. The resulting T-values, representing edge PC development in term-born infants, were visualized in Fig. 6A. Additionally, we quantified the edge-wise co-expression amplitude for each gene as the product of its expression levels in paired regions (Fig. 6B).

To identify genes significantly correlated with edge PC development, we performed Pearson's correlation between edge-wise T-values and co-expression amplitudes. We applied a permutation test by first reshaping the edge-wise T-values into a matrix, and randomly permuting its rows before vectorizing the upper triangle. This procedure was repeated 50,000 times to generate a null distribution of correlation coefficients. The permutation-derived P-value (referred to as P_{perm} in the main text) was obtained by comparing the observed coefficient with this null distribution (two-sided). Significantly correlated genes ($P_{perm} < 0.001$) were ranked in descending order according to their correlation coefficients and subsequently subjected to Gene Ontology (GO) enrichment analysis using Metascape (https://metascape.org). GO terms were deemed significant at FDR-corrected $P < 0.05$ using the Benjamini–Hochberg procedure. The remaining significant terms were then hierarchically clustered based on Kappa-statistical similarities, with a 0.3 Kappa score threshold applied[91].

Following the approach in Li et al.[53], we then performed Gene set enrichment analysis (GSEA) to assess enrichment in typical neurodevelopmental processes and neuronal metabolic pathways, using the clusterProfiler (https://bioconductor.org/packages/release/bioc/html/clusterProfiler.html) and enrichplot (https://bioconductor.org/packages/release/bioc/html/enrichplot.html) packages. The statistical significance of the enrichment score (ES) was assessed using permutation tests by randomly shuffling the phenotype labels 10,000 times. To account for gene set size differences, we computed a normalized enrichment score (NES) by dividing the observed ES by the mean ES from the permutation distribution. This normalization allowed for robust comparison across gene sets of varying sizes.

Cell type-specific analysis

Following the procedure in Seidlitz et al.[92], we classified cell types into seven canonical categories: microglia, endothelial cells, oligodendrocyte precursors, oligodendrocytes, astrocytes, excitatory, and inhibitory neurons. We then assessed the enrichment of our selected gene set across these cell types by computing the overlap with each category. The P-value of overlap was determined by a permutation test[93], and FDR-corrected using the Benjamini–Hochberg method.

Statistics and reproducibility

Statistical comparisons made between eight cognitive systems were implemented using one-way analysis of variance (ANOVA). Pairwise comparisons of group-level whole-brain distributions were performed using two-sample t-tests at each node or edge, with P-values corrected for multiple comparisons using the Benjamini–Hochberg method (FDR correction). System-level comparisons of within- and between-system edge PC were examined using paired t-tests, with P-values corrected for multiple comparisons using the Benjamini–Hochberg method (FDR correction). To reveal group differences in functional diversity across three groups (PT1: $n = 152$, PT2: $n = 135$, FT: $n = 494$), a linear mixed effect (LME) model was applied to control for potential confounding variables, including GA at birth, sex, birth weight and head motion (calculated as mean DVARS). F-values reflecting group effects were then estimated using ANOVA and thresholded at $P < 0.01$ after Bonferroni correction for multiple comparisons. The developmental effects of edge PC were assessed using a general linear model (GLM), with GA at birth, sex, birth weight, and head motion included as covariates, and P-values corrected for multiple comparisons using the Bonferroni method.

To better explore and visualize the dynamic growth patterns of edge PC, we applied a PMA-dependent sliding window approach in both full-term and preterm groups. All full-term infants were first ranked in ascending order based on their PMA at scan. A window length of 20 infants with a sliding step size of 10 was chosen (i.e., infants 1–20 in window1, infants 11–30 in window 2… infants (10N-9) to 10(N+1) in window N). This resulted in 47 overlapping subgroups in the full-term group, with a mean within-window PMA at scan ranging from 38.12 to 44.02 weeks. For preterm groups, which included infants scanned both at TEA and before TEA, a total of 27 overlapping subgroups were generated, with mean within-window PMA at scan ranging from 29.29 to 43.44 weeks. This approach enabled a qualitative examination of the dynamic fluctuations in edge PC with increasing age during infancy.

Reporting summary

Further information on research design is available in the Nature Portfolio Reporting Summary linked to this article.

Data availability

The imaging and collateral data used in this study were included in the 2021 (third) dHCP data release, which can be downloaded by registering at https://data.developingconnectome.org/. The BrainSpan Atlas is freely available at https://www.BrainSpan.org/static/download.html/. Source data underlying Figs. 1–6 can be accessed at https://figshare.com/articles/dataset/ePC_dHCP_data_source/29664158[94].

Code availability

This study used openly available software and codes. The code to compute eFC and its related derivatives is available at https://github.com/brain-networks[28]. The Brain Connectivity Toolbox is freely available online:

https://sites.google.com/site/bctnet/. The brain maps were presented using BrainNet Viewer v1.7 (https://www.nitrc.org/projects/bnv/). The code relevant to this study can be accessed at https://github.com/TianyuFang2000/ePC_master.

Received: 7 April 2025; Accepted: 9 September 2025;
Published online: 14 October 2025

References

1. Bethlehem, R. A. I. et al. Brain charts for the human lifespan. *Nature* **604**, 525–533 (2022).
2. Gilmore, J. H., Knickmeyer, R. C. & Gao, W. Imaging structural and functional brain development in early childhood. *Nat. Rev. Neurosci.* **19**, 123–137 (2018). *2018 19:3*.
3. Gao, W., Lin, W., Grewen, K. & Gilmore, J. H. Functional connectivity of the infant human brain: plastic and modifiable. *Neuroscientist* **23**, 169–184 (2017).
4. Alcauter, S. et al. Frequency of spontaneous BOLD signal shifts during infancy and correlates with cognitive performance. *Dev. Cogn. Neurosci.* **12**, 40–50 (2015).
5. Gao, W. et al. Evidence on the emergence of the brain's default network from 2-week-old to 2-year-old healthy pediatric subjects. *Proc. Natl Acad. Sci. USA* **106**, 6790–6795 (2009).
6. Ouyang, M., Dubois, J., Yu, Q., Mukherjee, P. & Huang, H. Delineation of early brain development from fetuses to infants with diffusion MRI and beyond. *Neuroimage* **185**, 836–850 (2019).
7. Elam, J. S. et al. The Human Connectome Project: a retrospective. *Neuroimage* **244**, 118543 (2021).
8. Karolis, V. R. et al. Maturational networks of human fetal brain activity reveal emerging connectivity patterns prior to ex-utero exposure. *Commun. Biol.* **6**, 661 (2023).
9. Hwang, K., Hallquist, M. N. & Luna, B. The development of hub architecture in the human functional brain network. *Cereb. Cortex* **23**, 2380–2393 (2013).
10. Wen, X. et al. First-year development of modules and hubs in infant brain functional networks. *Neuroimage* **185**, 222–235 (2019).
11. Chen, M. & Deem, M. W. Development of modularity in the neural activity of children's brains. *Biophys. J.* **106**, 795a (2014).
12. Nishimura, T., Takei, N., Tsuchiya, K. J., Asano, R. & Mori, N. Identification of neurodevelopmental trajectories in infancy and of risk factors affecting deviant development: a longitudinal birth cohort study. *Int. J. Epidemiol.* **45**, 543–553 (2016).
13. Hutchison, R. M. & Morton, J. B. Tracking the brain's functional coupling dynamics over development. *J. Neurosci.* **35**, 6849–6859 (2015).
14. Thion, M. S., Ginhoux, F. & Garel, S. Microglia and early brain development: an intimate journey. *Science* **362**, 185–189 (2018).
15. Gao, W., Alcauter, S., Smith, J. K., Gilmore, J. H. & Lin, W. Development of human brain cortical network architecture during infancy. *Brain Struct. Funct.* **220**, 1173–1186 (2015).
16. Johnson, M. H. Functional brain development in humans. *Nat. Rev. Neurosci.* **2**, 475–483 (2001).
17. Lewis, M. D. Self-organizing individual differences in brain development. *Dev. Rev.* **25**, 252–277 (2005).
18. Stoecklein, S. et al. Variable functional connectivity architecture of the preterm human brain: Impact of developmental cortical expansion and maturation. *Proc. Natl Acad. Sci. USA* **117**, 1201–1206 (2020).
19. Schafer, D. P. et al. Microglia sculpt postnatal neural circuits in an activity and complement-dependent manner. *Neuron* **74**, 691–705 (2012).
20. Zheng, W., Wang, X., Liu, T., Hu, B. & Wu, D. Preterm-birth alters the development of nodal clustering and neural connection pattern in brain structural network at term-equivalent age. *Hum. Brain Mapp.* **44**, 5372–5386 (2023).
21. Fenn-Moltu, S. et al. Development of neonatal brain functional centrality and alterations associated with preterm birth. *Cereb. Cortex* **33**, 5585–5596 (2023).
22. Shi, R. et al. Gene-environment interactions in the influence of maternal education on adolescent neurodevelopment using ABCD study. *Sci. Adv.* **10**, eadp3751 (2024).
23. Xia, Y. et al. Development of sensorimotor-visual connectome gradient at birth predicts neurocognitive outcomes at 2 years of age. *iScience* **27**, 108981 (2024).
24. Liu, J., Chen, H., Cornea, E., Gilmore, J. H. & Gao, W. Longitudinal developmental trajectories of functional connectivity reveal regional distribution of distinct age effects in infancy. *Cereb. Cortex* **33**, 10367–10379 (2023).
25. Bagonis, M. et al. Early childhood development of node centrality in the white matter connectome and its relationship to IQ at age 6 years. *Biol. Psychiatry Cogn. Neurosci. Neuroimaging* **8**, 1024–1032 (2023).
26. Hong, Y. et al. Structural and functional connectome relationships in early childhood. *Dev. Cogn. Neurosci.* **64**, 101314 (2023).
27. Ji, L. et al. Trajectories of human brain functional connectome maturation across the birth transition. *PLoS Biol.* **22**, e3002909 (2024).
28. Faskowitz, J., Esfahlani, F. Z., Jo, Y., Sporns, O. & Betzel, R. F. Edge-centric functional network representations of human cerebral cortex reveal overlapping system-level architecture. *Nat. Neurosci.* **23**, 1644–1654 (2020).
29. Esfahlani, F. Z. et al. High-amplitude cofluctuations in cortical activity drive functional connectivity. *Proc. Natl Acad. Sci. USA* **117**, 28393–28401 (2020).
30. Jo, Y. et al. The diversity and multiplexity of edge communities within and between brain systems. *Cell Rep.* **37**, 110032 (2021).
31. Sporns, O., Faskowitz, J., Teixeira, A. S., Cutts, S. A. & Betzel, R. F. Dynamic expression of brain functional systems disclosed by fine-scale analysis of edge time series. *Netw. Neurosci.* **5**, 405–433 (2021).
32. Betzel, R. F., Cutts, S. A., Greenwell, S., Faskowitz, J. & Sporns, O. Individualized event structure drives individual differences in whole-brain functional connectivity. *Neuroimage* **252**, 118993 (2022).
33. Jo, Y., Faskowitz, J., Esfahlani, Z., Sporns, O. & Betzel, R. F. Subject identification using edge-centric functional connectivity. *Neuroimage* **238**, 118204 (2021).
34. Gao, W. et al. Functional network development during the first year: relative sequence and socioeconomic correlations. *Cereb. Cortex* **25**, 2919–2928 (2015).
35. Li, M. et al. Integrative functional genomic analysis of human brain development and neuropsychiatric risks. *Science***362**, eaat7615 (2018).
36. Miller, J. A. et al. Transcriptional landscape of the prenatal human brain. *Nature* **508**, 199–206 (2014).
37. Sporns, O. The human connectome: origins and challenges. *Neuroimage* **80**, 53–61 (2013).
38. Cao, M., Huang, H. & He, Y. Developmental connectomics from infancy through early childhood. *Trends Neurosci.* **40**, 494–506 (2017).
39. Dimitrova, R. et al. Heterogeneity in brain microstructural development following preterm birth. *Cereb. Cortex* **30**, 4800–4810 (2020).
40. Malak, R. et al. Application of the neonatal behavioral assessment scale to evaluate the neurobehavior of preterm neonates. *Brain Sci.* **11**, 1285 (2021).
41. Dimitrova, R. et al. Phenotyping the preterm brain: characterizing individual deviations from normative volumetric development in two large infant cohorts. *Cereb. Cortex* **31**, 3665–3677 (2021).
42. Thompson, D. K. et al. Characterization of the corpus callosum in very preterm and full-term infants utilizing MRI. *Neuroimage* **55**, 479–490 (2011).

43. Büchel, C. & Friston, K. J. Modulation of connectivity in visual pathways by attention: cortical interactions evaluated with structural equation modelling and fMRI. *Cereb. Cortex* **7**, 768–778 (1997).
44. McLaughlin, K. A., Weissman, D. & Bitrán, D. Childhood adversity and neural development: a systematic review. *Annu. Rev. Dev. Psychol.* **1**, 277–312 (2019).
45. Wu, Q. et al. Modes of effective connectivity within cortical pathways are distinguished for different categories of visual context: an fMRI study. *Front. Behav. Neurosci.* **11**, 64 (2017).
46. Bijsterbosch, J. D., Valk, S. L., Wang, D. & Glasser, M. F. Recent developments in representations of the connectome. *Neuroimage* **243**, 118533 (2021).
47. Cosme, D. et al. Testing the adolescent social reorientation model during self and other evaluation using hierarchical growth curve modeling with parcellated fMRI data. *Dev. Cogn. Neurosci.* **54**, 101089 (2022).
48. Sheridan, M. A. & McLaughlin, K. A. Dimensions of early experience and neural development: Deprivation and threat. *Trends Cogn. Sci.* **18**, 580–585 (2014).
49. Zhang, H., Yin, W., Lin, W. & Shen, D. Early brain functional segregation and integration predict later cognitive performance. In *Connectomics in NeuroImaging* (eds Wu, G., Laurienti, P., Bonilha, L. & Munsell, B. C.) 116–124 (Springer International Publishing, Cham, 2017).
50. Baum, G. L. et al. Modular Segregation of Structural Brain Networks Supports the Development of Executive Function in Youth. *Curr. Biol.* **27**, 1561–1572.e8 (2017).
51. Yin, W. et al. The emergence of a functionally flexible brain during early infancy. *Proc. Natl Acad. Sci. USA* **117**, 23904–23913 (2020).
52. Cao, M. et al. Early development of functional network segregation revealed by connectomic analysis of the preterm human brain. *Cereb. Cortex* **27**, 1949–1963 (2017).
53. Li, Q. et al. Development of segregation and integration of functional connectomes during the first 1,000 days. *Cell Rep.* **43**, 114168 (2024).
54. Yu, X. et al. Functional connectivity in infancy and toddlerhood predicts long-term language and preliteracy outcomes. *Cereb. Cortex* **32**, 725–736 (2022).
55. Emerson, R. W., Gao, W. & Lin, W. Longitudinal study of the emerging functional connectivity asymmetry of primary language regions during infancy. *J. Neurosci.* **36**, 10883–10892 (2016).
56. Nosarti, C. et al. Preterm birth and psychiatric disorders in young adult life. *Arch. Gen. Psychiatry* **69**, 610–617 (2012).
57. Bouyssi-Kobar, M., De Asis-Cruz, J., Murnick, J., Chang, T. & Limperopoulos, C. Altered functional brain network integration, segregation, and modularity in infants born very preterm at term-equivalent age. *J. Pediatrics* **213**, 13–21.e1 (2019).
58. Van Den Heuvel, M. P. et al. The neonatal connectome during preterm brain development. *Cereb. Cortex* **25**, 3000–3013 (2015).
59. Ball, G. et al. Multimodal image analysis of clinical influences on preterm brain development. *Ann. Neurol.* **82**, 233–246 (2017).
60. Smyser, C. D. & Neil, J. J. Use of resting-state functional MRI to study brain development and injury in neonates. *Semin. Perinatol.* **39**, 130–140 (2015).
61. Mink, J. W., Blumenschine, R. J. & Adams, D. B. Ratio of central nervous system to body metabolism in vertebrates: Its constancy and functional basis. *Am. J. Physiol. Regul. Integr. Comp. Physiol.* **10**, 203–212 (1981).
62. Zlokovic, B. V. & Apuzzo, M. L. J. Strategies to circumvent vascular barriers of the central nervous system. *Neurosurgery* **43**, 877–878 (1998).
63. Wälchli, T. et al. Quantitative assessment of angiogenesis, perfused blood vessels and endothelial tip cells in the postnatal mouse brain. *Nat. Protoc.* **10**, 53–74 (2015).
64. Dingezweni, S. The blood–brain barrier. *South. Afr. J. Anaesth. Analgesia* **26**, S32–S34 (2020).
65. Kadry, H., Noorani, B. & Cucullo, L. A blood–brain barrier overview on structure, function, impairment, and biomarkers of integrity. *Fluids Barriers CNS* **17**, 69 (2020).
66. Goasdoué, K., Miller, S. M., Colditz, P. B. & Björkman, S. T. Review: The blood-brain barrier; protecting the developing fetal brain. *Placenta* **54**, 111–116 (2017).
67. Gilmore, J. H. et al. Early postnatal development of corpus callosum and corticospinal white matter assessed with quantitative tractography. *Am. J. Neuroradiol.* **28**, 1789–1795 (2007).
68. Knickmeyer, R. C. et al. A structural MRI study of human brain development from birth to 2 years. *J. Neurosci.* **28**, 12176–12182 (2008).
69. Geng, X. et al. White matter heritability using diffusion tensor imaging in neonatal brains. *Twin Res. Hum. Genet.* **15**, 336–350 (2012).
70. Tau, G. Z. & Peterson, B. S. Normal development of brain circuits. *Neuropsychopharmacology* **35**, 147–168 (2010).
71. Friston, K. J. Functional and effective connectivity: a review. *Brain Connect* **1**, 13–36 (2011).
72. Newman, M. E. J. & Girvan, M. Finding and evaluating community structure in networks. *Phys. Rev. E* **69**, 026113 (2004).
73. Rosvall, M. & Bergstrom, C. T. Maps of random walks on complex networks reveal community structure. *Proc. Natl Acad. Sci. USA* **105**, 1118–1123 (2008).
74. Fortunato, S. Community detection in graphs. *Phys. Rep.* **486**, 75–174 (2010).
75. Hyvärinen, A. & Oja, E. Independent component analysis: algorithms and applications. *Neural Netw.* **13**, 411–430 (2000).
76. Beckmann, C. F., DeLuca, M., Devlin, J. T. & Smith, S. M. Investigations into resting-state connectivity using independent component analysis. *Philos. Trans. R. Soc. B: Biol. Sci.* **360**, 1001–1013 (2005).
77. Volpe, J. J. Brain injury in premature infants: a complex amalgam of destructive and developmental disturbances. *Lancet Neurol.* **8**, 110–124 (2009).
78. Hintz, S. R. et al. Neuroimaging and neurodevelopmental outcome in extremely preterm infants. *Pediatrics* **135**, e32–e42 (2015).
79. Woodward, L. J., Anderson, P. J., Austin, N. C., Howard, K. & Inder, T. E. Neonatal MRI to predict neurodevelopmental outcomes in preterm infants. *N. Engl. J. Med.* **355**, 685–694 (2006).
80. Boardman, J. P. et al. Early growth in brain volume is preserved in the majority of preterm infants. *Ann. Neurol.* **62**, 185–192 (2007).
81. Edwards, A. D. et al. The developing Human Connectome Project Neonatal Data Release. *Front Neurosci.* **16**, 886772 (2022).
82. Aylward, G. P. Bayley scales of infant and toddler development. In *Encyclopedia of Clinical Neuropsychology* (eds Kreutzer, J. S., DeLuca, J. & Caplan, B.) 519–521 (Springer International Publishing, Cham, 2018).
83. Hughes, E. J. et al. A dedicated neonatal brain imaging system. *Magn. Reson. Med.* **78**, 794–804 (2017).
84. Fitzgibbon, S. P. et al. The developing Human Connectome Project (dHCP) automated resting-state functional processing framework for newborn infants. *Neuroimage* **223**, 117303 (2020).
85. Jenkinson, M., Beckmann, C. F., Behrens, T. E. J., Woolrich, M. W. & Smith, S. M. Review FSL. *Neuroimage* **62**, 782–790 (2012).
86. Shi, F. et al. Infant brain atlases from neonates to 1- and 2-year-olds. *PLoS ONE* **6**, e18746 (2011).
87. Avants, B. B. et al. A reproducible evaluation of ANTs similarity metric performance in brain image registration. *Neuroimage* **54**, 2033–2044 (2011).
88. Thomas Yeo, B. T. et al. The organization of the human cerebral cortex estimated by intrinsic functional connectivity. *J. Neurophysiol.* **106**, 1125–1165 (2011).
89. Denisova, K. Neurobiology, not artifacts: challenges and guidelines for imaging the high risk infant. *Neuroimage* **185**, 624–640 (2019).

90. Cox, R. W. AFNI: Software for analysis and visualization of functional magnetic resonance neuroimages. *Comput. Biomed. Res.* **29**, 162–173 (1996).
91. Zhou, Y. et al. Metascape provides a biologist-oriented resource for the analysis of systems-level datasets. *Nat. Commun.* **10**, 1523 (2019).
92. Seidlitz, J. et al. Transcriptomic and cellular decoding of regional brain vulnerability to neurogenetic disorders. *Nat. Commun.* **11**, 3358 (2020).
93. Romero-Garcia, R. et al. Schizotypy-related magnetization of cortex in healthy adolescence is colocated with expression of Schizophrenia-related genes. *Biol. Psychiatry* **88**, 248–259 (2020).
94. Fang, T. ePC_dHCP_development [Dataset]. *Figshare* https://doi.org/10.6084/m9.figshare.29664158.v3 (2025).
95. Xia, M., Wang, J. & He, Y. BrainNet Viewer: a network visualization tool for human brain connectomics. *PLoS ONE* **8**, e68910 (2013).

Acknowledgements

We would like to acknowledge the Developing Human Connectome Project for granting access to neonatal fMRI data, which was instrumental in our analysis. This work was supported by the National Natural Science Foundation of China (82202249, 82071994).

Author contributions

T.Y.F. and Y.Y.C. proposed the concept and designed the research. W.J.L., R.W. and Y.Z. provided the methodological instruction. T.Y.F. and Y.Y.C. performed the data analyses and interpreted the findings. Y.Y.C., Q.Y.F., X.Z., D.M., Y.G. and Y.C.H. supervised the experiments. T.Y.F. and Y.Y.C. wrote the manuscript. Y.Y.C., Q.Y.F. and D.M. revised the manuscript.

Competing interests

The authors declare no competing interests.

Additional information

Supplementary information The online version contains supplementary material available at https://doi.org/10.1038/s42003-025-08873-4.

Correspondence and requests for materials should be addressed to Yuanyuan Chen, Qiuyun Fan or Dong Ming.

Peer review information *Communications Biology* thanks Kevin Cook and the other, anonymous, reviewer(s) for their contribution to the peer review of this work. Primary Handling Editors: Sahar Ahmad and Jasmine Pan. A peer review file is available.